Quasimonoenergetic Proton Bunch Acceleration Driven by Hemispherically Converging Collisionless Shock in a Hydrogen Cluster Coupled with Relativistically Induced Transparency

Ryutaro Matsui,[1,2] Yuji Fukuda,[2,*] and Yasuaki Kishimoto[1,†]
[1]*Graduate School of Energy Science, Kyoto University, Gokasho, Uji, Kyoto 611-0011, Japan*
[2]*Kansai Photon Science Institute (KPSI), National Institutes for Quantum and Radiological Science and Technology (QST), 8-1-7 Umemidai, Kizugawa, Kyoto 619-0215, Japan*

(Received 31 March 2018; published 10 January 2019)

An approach for accelerating a quasimonoenergetic proton bunch via a hemispherically converging collisionless shock created in laser-cluster interactions at the relativistically induced transparency (RIT) regime is studied using three-dimensional particle-in-cell simulations. By the action of focusing a petawatt class laser pulse onto a micron-size spherical hydrogen cluster, a crescent-shaped collisionless shock is launched at the laser-irradiated hemisphere and propagates inward. The shock converges at the sphere center in concurrence with the onset of the RIT, thereby allowing the proton bunch to be pushed out from the shock surface in the laser propagation direction. The proton bunch experiences further acceleration both inside and outside of the cluster to finally exhibit a quasimonoenergetic spectral peak around 300 MeV while maintaining a narrow energy spread (∼10%) and a small half-divergence angle (∼5°) via the effect of the RIT. This mechanism works for finite ranges of parameters with threshold values concerning the laser peak intensity and the cluster radius, resulting from the synchronization of the multiple processes in a self-consistent manner. The present scheme utilizing the internal and external degrees of freedom ascribed to the spherical cluster leads to the proton bunch alternative to the plain target, which allows the operation with a high repetition rate and impurity free.

DOI: 10.1103/PhysRevLett.122.014804

Laser plasma ion acceleration is characterized by its large accelerating field gradient and has been extensively studied over the past decade [1,2]. This is because resultant ion beams have unique properties, such as ultrashort duration, high brilliance, and low emittance, that explore a broad range of applications, including proton radiography [3], hadron therapy [4,5], nuclear science [6,7], fast ignition [8,9], isochoric heating of matter [10], and radiation-induced processes in matter [11].

The recent advancements in both laser and target fabrication techniques have led to the enhancement of the accelerated proton cutoff energies close to 100 MeV [12–14]. However, the energy spectra show a wide spread, which reduces the effective beam current to be utilized. In addition, lower angular divergence of accelerated ions and also higher repetition rates, which are technological issues using solid thin film targets, are requested for the wider use of this scheme.

Several schemes have so far been proposed to explain experimental results and to explore further efficient acceleration. The target normal sheath acceleration [15] is a well-known mechanism. However, the scheme generally exhibits broad exponential energy spectra with wide angular divergence. Considerable efforts have been made to obtain a narrow energy spectrum via the engineering of target structures [16,17], the development of the isolated sphere target [18,19], and the exploration of advanced acceleration mechanisms including the radiation pressure acceleration [20–25], the breakout afterburner [26], and the collisionless shock acceleration (CSA) [27–34]. In most of these cases, however, the results are either preliminary or require further confirmation. In order to widen the possibility for high energy proton acceleration which simultaneously satisfies the requirements mentioned above, here, we consider a different approach using micron-size spherical hydrogen clusters, alternative to that using solid thin film targets.

The interaction of cluster targets, composed of nanometer-micrometer-size clusters and ambient gas, with intense laser pulses has been actively researched for over 20 years [35,36] because the cluster targets allow very efficient coupling with laser pulses compared with solid targets [37–39] even in the radiation dominant regime [40]. The pioneering experimental works in the 1990s of generating bright x rays [41] and MeV-class multiply charged ions [42] from Coulomb exploding high-Z clusters and fusion neutrons from Coulomb exploding deuterium clusters [43] have attracted wide attention. These are attributed to collective electron dynamics in individual clusters. On the other hand, the cluster targets act as efficient nonlinear

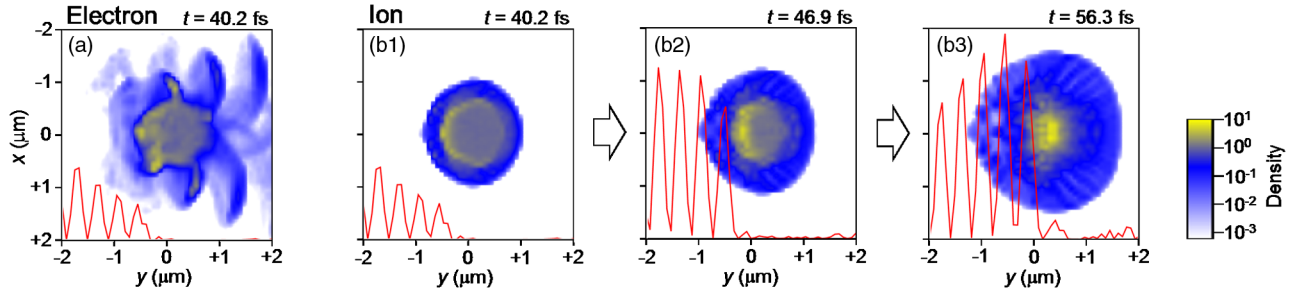

FIG. 1. 2D images of (a) electron and (b1)–(b3) ion density distributions for $R_0 = 0.8$ μm in the x-y plane at $z = 0$ at different times. The densities are shown as an averaged value over $z = 0 \pm 0.16$ μm and are normalized by the initial density of the cluster ions or electrons n_0. The intensities of the laser electric fields E_x^2 along the y axis are shown in red lines.

media for the self-focusing of an incident laser pulse [44], leading to the formation of a self-guided plasma channel [45] and a plasma filament [46], which are closely connected with the recent remarkable studies including enhanced soft x-ray generation [47] and multi-MeV ion acceleration [48], high-charge sub-GeV electron acceleration [49], bright keV betatron x rays [50], MeV-energy neutral atoms [51], and nonlocal electron transport in radiative blast wave [52].

In this Letter, we present a new scheme which applies such prominent characteristics of cluster targets for achieving quasimonoenergetic proton bunch acceleration with a low angular divergence by utilizing the internal degree of freedom (d.o.f.). In this scheme, the collisionless shock dynamics inside the micron-size cluster subsequently coupled with relativistically induced transparency (RIT) [26,53,54] effect of high-intensity laser plays an important role. The external d.o.f. associated with the cluster expansion due to the sheath field is also incorporated. These multiple processes can be synchronized in a self-consistent manner once conditions for the laser and cluster are satisfied, leading to the quasimonoenergetic proton bunch acceleration.

Simulations are performed using a three-dimensional version of the particle-based integrated code EPIC3D [55]. The system size is $L_x \times L_y \times L_z = 10.24 \times 20.48 \times 10.24$ μm containing $128 \times 256 \times 128$ cells. A cell size of 80 nm is employed to resolve the shock ($\sim$0.40 μm) and associated electric field structures. A spherical hydrogen cluster is placed at the center of the box $(x, y, z) = (0, 0, 0)$, which consists of $\sim 10^{10}$ hydrogen molecules with the radius of $R_0 = 0.8$ μm and the electron density of $n_e = 4.6 \times 10^{22}$ cm$^{-3} = 26.8 n_c$. Here, n_c denotes the critical density of the plasma for the laser wavelength $\lambda = 0.81$ μm. Ambient hydrogen gas with $n_e = 4.0 \times 10^{19}$ cm$^{-3} = 0.024 n_c$ occupies the simulation box. The cluster is reproduced by particle-in-cell (PIC) particles using 6,730 per cell and a fully ionized plasma is assumed as the initial condition. A linearly polarized laser pulse in the x direction, with duration of $\tau = 33$ fs (FWHM) is chosen, is generated from an antenna located at $y = -4.96$ μm ($x = z = 0$) and propagates in the $+y$ direction. The peak intensity of the laser pulse is set to $I = 1.0 \times 10^{22}$ W/cm^2 (the normalized amplitude $a_0 = 69$). Here, the laser energy irradiated to the cross section of the cluster for $R_0 = 0.8$ μm is approximately 6.3 J. The periodic boundary condition is employed in the x and z directions, while the transparent boundary condition is employed in the y direction for the fields and particles. These parameters are employed based on the production of micron-size hydrogen clusters [56,57] and the achievement of 10^{22} W/cm^2 focused laser intensity [58,59]. In the following, we present the simulation results and explain the mechanisms [four phases labeled (A)–(D)].

Figure 1 shows the two-dimensional images of electron and ion density distributions for $R_0 = 0.8$ μm. When a leading edge of the laser pulse reaches the spherical cluster at $t = 40.2$ fs, the laser field expels electrons from the peripheral region of the cluster, which corresponds to the initial electron skin depth $\delta_e = 25$ nm, whereas most electrons remain inside the cluster core [Fig. 1(a)]. Here, δ_e includes the relativistic effect. The peripheral region of the cluster ($R_0 - \delta_e \le r \le R_0$) is positively charged and undergoes the anisotropic Coulomb explosion on a femtosecond-picosecond timescale due to the anisotropic density distribution of electrons [Fig. 1(a)] resulting from the strong magnetic field of laser ($\sim$900 kT), whereas the cluster core expands on a hydrodynamic timescale (picosecond-nanosecond).

Shock initiation and propagation (A).—As the laser intensity increases, a charge separation is induced at the surface of the laser-irradiated hemisphere via the action of the laser ponderomotive force f_p on the remaining core electrons, and then a crescent-shaped collisionless shock is launched [Fig. 1(b1)]. The shock propagates inward while maintaining the crescent shape [Fig. 1(b2)] and converges at the sphere center at $t = 56.3$ fs. Notably, the pulse peak also reaches the cluster center at this time [Fig. 1(b3)]. Here, the shock Mach number is calculated as $M_{\rm sh} = 1.3$ using the shock velocity $v_{\rm sh} = 0.20c$ and the ion-acoustic velocity $c_s = 0.15c$.

Collisionless shock acceleration (B).—Figure 2 shows the temporal evolution for the electron and ion densities

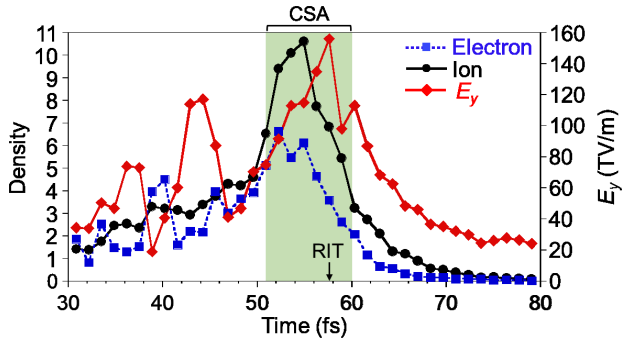

FIG. 2. Temporal evolution for the electron density (blue squares), the ion density (black circles), and the electric field E_y (red diamonds) inside the shock along the y axis at $x = z = 0$. The densities are normalized by n_0. The time region when the CSA occurs is colored green. The arrow indicates the time when the quasimonoenergetic proton bunch is pushed out via the RIT effect.

inside the shock, and for the electric field E_y associated with the shock. During the propagation of the shock, both the electron and ion densities inside the shock gradually increase because of the accumulation of the charged particles by the converging effect. Notably, after $t = 50.9$ fs, the ion density inside the shock sharply increases and largely exceeds the electron density. Generally, when the shock potential becomes larger than the kinetic energy of upstream ions in the shock-rest frame, a so-called CSA process starts. The shock front can produce quasimonoenergetic ions by reflecting upstream ions to double the shock velocity [27]. Indeed, at $t = 50.9$ fs, the shock potential (10 MeV) becomes larger than the kinetic energy of upstream protons (6.7 MeV) in the shock-rest frame, thereby enabling the CSA of upstream protons. The reflected upstream protons have the maximum velocity of $v_{\rm ion} = 2v_{\rm sh} - v_{\rm exp} = 0.27c$, corresponding to 33 MeV [Fig. 3(b1)]. Here, $v_{\rm exp}$ is the velocity of the upstream expanding protons preaccelerated by the front part of the shock potential.

RIT onset and acceleration (C).—At $t = 56.3$ fs, the pulse peak and the shock front reach the cluster center at the same time. After this moment, the effect of a so-called RIT [26,53,54] becomes dominant: The laser fields start to penetrate into the shock structure because δ_e becomes comparable to the thickness of the shock due to the relativistic effect, whereas the peak electron density inside the shock remains larger than a relativistic critical density $\gamma_e n_c$ [Fig. 3(c)]. Here, γ_e is defined as $\gamma_e = \sqrt{1 + a_0^2/2}$ for a linearly polarized laser pulse. As a result, a number of electrons inside the shock are rapidly heated and expelled in the longitudinal direction via f_p. Therefore, the electric field associated with the shock reaches a maximum and quickly decreases as shown in Fig. 2. Indeed, $v_{\rm sh}$ temporarily increases from $0.20c$ ($t = 56.3$ fs) up to $0.41c$ ($t = 57.6$ fs) and then recovers to $0.20c$ ($t = 58.9$ fs). During this process, quasimonoenergetic protons are pushed out from the shock surface as a bunch, which is highly localized in both longitudinal and transverse directions [Fig. 3(b2)]. Figure 3(d) shows the phase space distribution of cluster ions at $t = 58.9$ fs. The released bunch located at $y = +0.9$ μm has the maximum velocity of $v_{\rm ion} = 0.42c$, corresponding to 95 MeV.

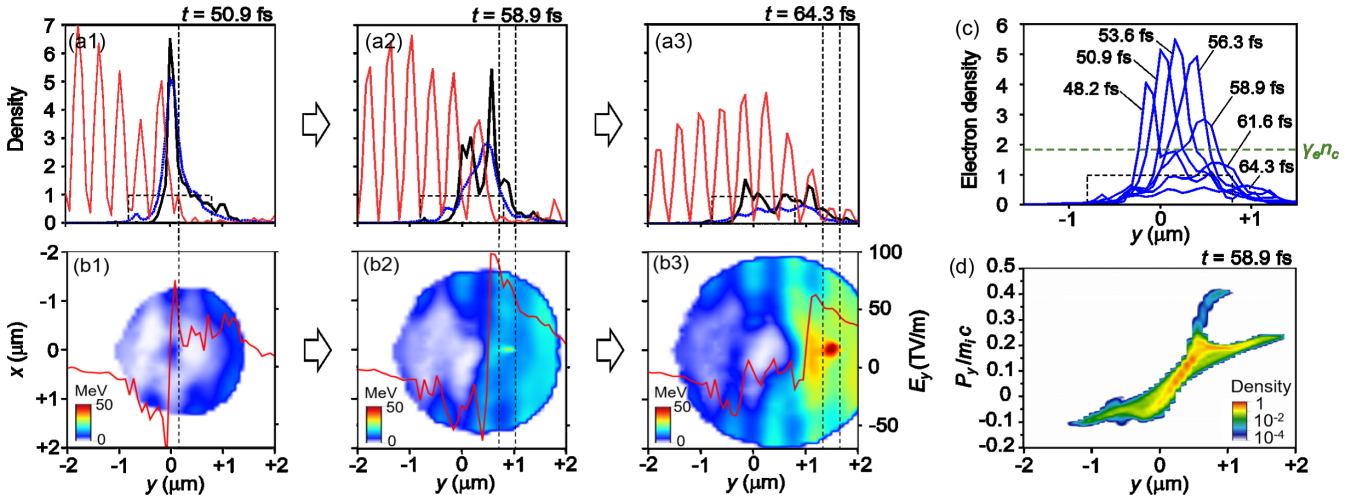

FIG. 3. (a1)–(a3),(c) One-dimensional cross-sectional views for the charge density distributions of the cluster ions (black lines) and cluster electrons (blue lines) and the intensities of the laser electric fields E_x^2 (red lines) along the y axis at $x = z = 0$ at different times. (b1)–(b3) 2D images of the kinetic energy distributions of cluster ions in the x-y plane at $z = 0$ at different times. The ion energies are shown as a value which is averaged in each cell and over $z = 0 \pm 0.16$ μm. The electric fields E_y are also shown as red lines. (d) The phase space distribution of the cluster ions along the y axis at $x = z = 0$ at $t = 58.9$ fs. The densities in (a1)–(a3), (c), and (d) are normalized by n_0. Rectangular broken lines in (a1)–(a3) and (c) represent n_0. The vertical broken lines in (a1)–(a3) and (b1)–(b3) represent the location of the quasimonoenergetic proton bunch.

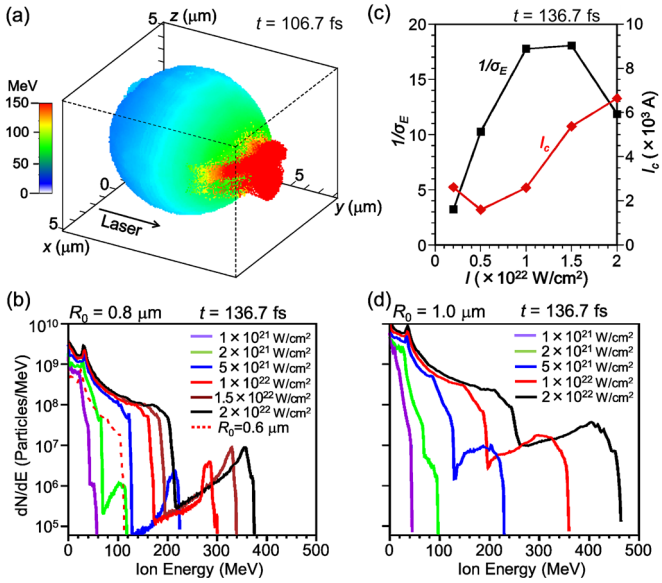

FIG. 4. (a) 3D image of the kinetic energy distribution of cluster ions at $t = 106.7$ fs. The quasimonoenergetic proton bunch (red) is flying out from the cluster. (b),(d) Proton energy spectra for clusters with (b) $R_0 = 0.8$ μm and (d) $R_0 = 1.0$ μm for various laser peak intensities at $t = 136.7$ fs. The spectrum for the cluster with $R_0 = 0.6$ μm at $t = 136.7$ fs is also shown as red dotted line in (b). The proton number is evaluated using a real value by multiplying the particle weight to the PIC particle. (c) The monochromaticity $1/\sigma_E$ (black square) and the current I_c (red diamond) for the bunch within σ_E.

Another important role of the RIT is its ability to enhance the monochromaticity of the bunch, which we define as $1/\sigma_E$ ($\sigma_E = \delta E/E$, energy spread), because the pushed-out protons having a higher velocity chase the leading protons, thereby causing the compression of the bunch. As will be discussed later, without the RIT effect, the monochromaticity becomes worse.

After the onset of the RIT, as shown in Fig. 3(c), the electron density inside the shock decreases drastically. The shock structure collapses and the intensity of E_y rapidly decreases with time (Fig. 2), leading to the end of the CSA at $t = 60.3$ fs. At this moment, the bunch is accelerated up to $0.45c$, corresponding to 108 MeV. After the CSA, as shown in Fig. 3(b3), the bunch is further accelerated by the remnant electric field of the shock inside the cluster. Over time, at $t = 75.8$ fs, the bunch reaches the cluster exploding front with $v_{\rm ion} = 0.60c$, corresponding to 211 MeV. At this moment, the velocity of the cluster exploding front in the $+y$ direction is $0.40c$; thus, the bunch flies out from the cluster with 4.3° half-divergence angle [Fig. 4(a)].

Sheath acceleration (D).—After leaving the cluster, the bunch is again further accelerated by the sheath electric field created by the Coulomb explosion of the cluster. At this acceleration stage, the maximum attainable energy of the bunch can be estimated as $K_{\rm max} = 300$ MeV, using the relation $K_{\rm max} = K_0 + \int_{r_0}^{\infty} eE(r)\,dr$, where $K_0 = 211$ MeV is the kinetic energy of the bunch at the cluster exploding front, r_0 is the distance of the cluster exploding front from the cluster center, and $E(r) \propto 1/r^2$ is the electric field of the Coulomb explosion outside of the cluster as a function of the distance r from the cluster center. In this study, the simulation has been performed up to $t = 136.7$ fs and the maximum kinetic energy of the bunch has a quasimonoenergetic peak at 290 MeV, which is close to the estimated maximum attainable kinetic energy, with an energy spread of $\sigma_E = \delta E/E \sim 7\%$ [red solid line in Fig. 4(b)]. Here, E is evaluated at the peak energy of the quasimonoenergetic component in the energy spectrum. The conversion efficiency of the irradiated laser energy into kinetic energy of protons is approximately 8.3% and that into kinetic energy of quasimonoenergetic protons is approximately 0.042%. Notably, the bunch energy 290 MeV is much larger than the maximum proton energy 170 MeV accelerated by the Coulomb explosion of the hydrogen cluster [red solid line in Fig. 4(b)].

The effect of the laser peak intensity I on the quasimonoenergetic proton bunch formation for $R_0 = 0.8$ μm is investigated in the range of 1.0×10^{21} to 2.0×10^{22} W/cm^2, which is shown in Fig. 4(b). The bunch (energy spread $\sigma_E \sim 10\%$) is found to be formed for $I > 2.0 \times 10^{21}$ W/cm^2. This indicates that the threshold value concerning the laser peak intensity exists for the multiple processes (A)–(D) to be synchronized, leading to the bunch formation. The threshold value roughly coincides with that causing the RIT, which is the driving force to compress the bunch at the shock surface. The energy [Fig. 4(b)] and the current I_c [Fig. 4(c)] for the bunch within σ_E increase with I. Notably, the bunch size increases with the current I_c due to the space-charge effect. The monochromaticity $1/\sigma_E$ also increases with I, reaching the maximum value around $I = (1.0$–$1.5) \times 10^{22}$ W/cm^2, while it decreases for further increase with I. These results show that the optimum laser peak intensity exists for the formation of the bunch with the maximum monochromaticity and current density.

The effect of the initial cluster radius is investigated by choosing $R_0 = 1.0$ μm in Fig. 4(d). The general tendency is similar to that for $R_0 = 0.8$ μm, indicating that the same acceleration mechanism is effective for $I > 2.0 \times 10^{21}$ W/cm^2. However, the monochromaticity becomes worse ($\sigma_E \sim 30\%$–40%). This is because the RIT occurs before the shock convergence at the cluster center, so that a slope of the electric field associated with the shock is less steep. Alternatively, in the smaller cluster case of $R_0 = 0.6$ μm, for $I = 1.0 \times 10^{22}$ W/cm^2, the bunch is not formed and the energy spectrum shows only the feature of the Coulomb explosion, i.e., the cutoff structure at 117 MeV [red dotted line in Fig. 4(b)]. This is because the height of the shock potential does not reach enough value to reflect upstream protons due to the limited mass of the cluster when the RIT occurs. As a result, the shock structure collapses before the onset of the CSA. This indicates that the threshold value concerning the cluster radius also exists.

The effect of the cluster electron density is also investigated while keeping $I = 1.0 \times 10^{22}$ W/cm^2. For the case of a carbon cluster with $R_0 = 0.8$ μm and $n_e = 2.8 \times 10^{23}$ cm^{-3}, the hemispherically converging collisionless shock is launched; however, it disappears before the onset of the CSA. Moreover, the RIT does not take place because $\gamma_e n_c = 8.3 \times 10^{22}$ cm^{-3} at the laser pulse peak is below n_e and δ_e also decreases compared with the hydrogen cluster case. Therefore, for the proposed ion acceleration mechanism to work, at least n_e should be below $\gamma_e n_c$ for a given laser peak intensity.

Finally, the preheating effect of the hydrogen cluster by the prepulse is considered. For $I = 1.0 \times 10^{22}$ W/cm^2, the prepulse with the contrast of 10^8–10^{10} [59] is considered to decrease the cluster size by approximately 10%. Based on this estimation, we performed simulations using a 0.7-μm radius cluster having the exponential decay around the surface and obtained high energy protons with a quasimonoenergetic peak ($\sigma_E \sim 10\%$) at 220 MeV. This indicates that the prepulse does not significantly affect the proposed acceleration mechanism for $R_0 \geq 0.8$ μm.

In conclusion, we presented a new scheme for achieving quasimonoenergetic proton acceleration by causing multiple processes created through the internal and external d.o.f. ascribed to the spherical structure of micron-size hydrogen cluster irradiated by high-intensity laser, i.e., (A)–(D), and by synchronizing their spatial-temporal evolutions. Based on the 3D relativistic PIC simulations, we demonstrated that produced proton bunches are accelerated to the level of 300 MeV while maintaining an energy spread around 10% and a low half-divergence angle around 5°. We found that the scheme stably works for finite ranges of parameters with threshold values, which is available for experiments. In order for the present scheme to deserve practical application, e.g., hadron therapy, further progresses about the manipulation and optimization of all-optical techniques and target fabrication are requested, which is ongoing work.

This work was supported by Grant-in-Aids for Scientific Research (A) No. 26247100, (A) No. 17H01180, and (B) No. 25287153 by JSPS.

*fukuda.yuji@qst.go.jp
†kishimoto@energy.kyoto-u.ac.jp

[1] H. Daido, M. Nishiuchi, and A. S Pirozhkov, Rep. Prog. Phys. **75**, 056401 (2012).
[2] A. Macchi, M. Borghesi, and M. Passoni, Rev. Mod. Phys. **85**, 751 (2013).
[3] M. Borghesi *et al.*, Phys. Plasmas **9**, 2214 (2002).
[4] S. V. Bulanov, T. Z. Esirkepov, V. S. Khoroshkov, A. V. Kuznetsov, and F. Pegoraro, Phys. Lett. A **299**, 240 (2002).
[5] V. Malka *et al.*, Med. Phys. **31**, 1587 (2004).
[6] K. W. D. Ledingham, P. McKenna, and R. P. Singhal, Science **300**, 1107 (2003).
[7] N. V. Zamfir, Eur. Phys. J. Spec. Top. **223**, 1221 (2014).
[8] M. Roth *et al.*, Phys. Rev. Lett. **86**, 436 (2001).
[9] Y. Kitagawa *et al.*, Phys. Rev. Lett. **114**, 195002 (2015).
[10] P. K. Patel, A. J. Mackinnon, M. H. Key, T. E. Cowan, M. E. Foord, M. Allen, D. F. Price, H. Ruhl, P. T. Springer, and R. Stephens, Phys. Rev. Lett. **91**, 125004 (2003).
[11] B. Dromey *et al.*, Nat. Commun. **7**, 10642 (2016).
[12] F. Wagner *et al.*, Phys. Rev. Lett. **116**, 205002 (2016).
[13] I. J. Kim *et al.*, Phys. Plasmas **23**, 070701 (2016).
[14] A. Higginson *et al.*, Nat. Commun. **9**, 724 (2018).
[15] S. C. Wilks, A. B. Langdon, T. E. Cowan, M. Roth, M. Singh, S. Hatchett, M. H. Key, D. Pennington, A. MacKinnon, and R. A. Snavely, Phys. Plasmas **8**, 542 (2001).
[16] B. M. Hegelich, B. J. Albright, J. Cobble, K. Flippo, S. Letzring, M. Paffett, H. Ruhl, J. Schreiber, R. K. Schulze, and J. C. Fernández, Nature (London) **439**, 441 (2006).
[17] H. Schwoerer, S. Pfotenhauer, O. Jäckel, K.-U. Amthor, B. Liesfeld, W. Ziegler, R. Sauerbrey, K. W. D. Ledingham, and T. Esirkepov, Nature (London) **439**, 445 (2006).
[18] S. Ter-Avetisyan *et al.*, Phys. Plasmas **19**, 073112 (2012).
[19] T. M. Ostermayr *et al.*, Phys. Rev. E **94**, 033208 (2016).
[20] T. Esirkepov, M. Borghesi, S. V. Bulanov, G. Mourou, and T. Tajima, Phys. Rev. Lett. **92**, 175003 (2004).
[21] B. Qiao, M. Zepf, M. Borghesi, and M. Geissler, Phys. Rev. Lett. **102**, 145002 (2009).
[22] A. Macchi, S. Veghini, and F. Pegoraro, Phys. Rev. Lett. **103**, 085003 (2009).
[23] A. Henig *et al.*, Phys. Rev. Lett. **103**, 245003 (2009).
[24] S. Kar *et al.*, Phys. Rev. Lett. **109**, 185006 (2012).
[25] S. Steinke *et al.*, Phys. Rev. ST Accel. Beams **16**, 011303 (2013).
[26] S. Palaniyappan, C. Huang, D. C. Gautier, C. E. Hamilton, M. A. Santiago, C. Kreuzer, A. B. Sefkow, R. C. Shah, and J. C. Fernández, Nat. Commun. **6**, 10170 (2015).
[27] L. O. Silva, M. Marti, J. R. Davies, R. A. Fonseca, C. Ren, F. S. Tsung, and W. B. Mori, Phys. Rev. Lett. **92**, 015002 (2004).
[28] F. Fiuza, A. Stockem, E. Boella, R. A. Fonseca, L. O. Silva, D. Haberberger, S. Tochitsky, C. Gong, W. B. Mori, and C. Joshi, Phys. Rev. Lett. **109**, 215001 (2012).
[29] H. Zhang *et al.*, Phys. Plasmas **22**, 013113 (2015).
[30] W. L. Wang, B. Qiao, T. W. Huang, X. F. Shen, W. Y. You, X. Q. Yan, S. Z. Wu, C. T. Zhou, and X. T. He, Phys. Plasmas **23**, 073118 (2016).
[31] C. A. J. Palmer *et al.*, Phys. Rev. Lett. **106**, 014801 (2011).
[32] D. Haberberger, S. Tochitsky, F. Fiuza, C. Gong, R. A. Fonseca, L. O. Silva, W. B. Mori, and C. Joshi, Nat. Phys. **8**, 95 (2012).
[33] S. N. Chen *et al.*, Sci. Rep. **7**, 13505 (2017).
[34] H. Zhang *et al.*, Phys. Rev. Lett. **119**, 164801 (2017).
[35] J. Posthumus, *Molecules and Clusters in Intense Laser Fields* (Cambridge University Press, Cambridge, England, 2009).
[36] T. Fennel, K.-H. Meiwes-Broer, J. Tiggesbäumker, P.-G. Reinhard, P. M. Dinh, and E. Suraud, Rev. Mod. Phys. **82**, 1793 (2010).
[37] T. Ditmire, R. A. Smith, J. W. G. Tisch, and M. H. R. Hutchinson, Phys. Rev. Lett. **78**, 3121 (1997).
[38] T. Tajima, Y. Kishimoto, and M. C. Downer, Phys. Plasmas **6**, 3759 (1999).

[39] Y. Kishimoto, T. Masaki, and T. Tajima, Phys. Plasmas **9**, 589 (2002).
[40] N. Iwata, H. Nagatomo, Y. Fukuda, R. Matsui, and Y. Kishimoto, Phys. Plasmas **23**, 063115 (2016).
[41] A. McPerson, B. D. Thompson, A. B. Borisov, K. Boyer, and C. K. Rhodes, Nature (London) **370**, 631 (1994).
[42] T. Ditmire, J. W. G. Tisch, E. Springate, M. B. Mason, N. Hay, R. A. Smith, J. Marangos, and M. H. R. Hutchinson, Nature (London) **386**, 54 (1997).
[43] T. Ditmire, J. Zweiback, V. P. Yanovsky, T. E. Cowan, G. Hays, and K. B. Wharton, Nature (London) **398**, 489 (1999).
[44] I. Alexeev, T. M. Antonsen, K. Y. Kim, and H. M. Milchberg, Phys. Rev. Lett. **90**, 103402 (2003).
[45] K. Y. Kim, H. M. Milchberg, A. Y. Faenov, A. I. Magunov, T. A. Pikuz, and I. Yu. Skobelev, Phys. Rev. E **73**, 066403 (2006).
[46] M. McCormick, A. V. Arefiev, H. J. Quevedo, R. D. Bengtson, and T. Ditmire, Phys. Rev. Lett. **112**, 045002 (2014).
[47] Y. Fukuda *et al.*, Appl. Phys. Lett. **92**, 121110 (2008).
[48] Y. Fukuda *et al.*, Phys. Rev. Lett. **103**, 165002 (2009).
[49] L. Zhang *et al.*, Appl. Phys. Lett. **100**, 014104 (2012).
[50] L. M. Chen *et al.*, Sci. Rep. **3**, 1912 (2013).
[51] R. Rajeev, T. M. Trivikram, K. P. M. Rishad, V. Narayanan, E. Krishnakumar, and M. Krishnamurthy, Nat. Phys. **9**, 185 (2013).
[52] A. Marocchino *et al.*, Appl. Phys. Lett. **112**, 264104 (2018).
[53] S. Palaniyappan *et al.*, Nat. Phys. **8**, 763 (2012).
[54] J. Fernández *et al.*, Phys. Plasmas **24**, 056702 (2017).
[55] Y. Kishimoto and T. Masaki, J. Plasma Phys. **72**, 971 (2006).
[56] S. Jinno *et al.*, Opt. Express **25**, 18774 (2017).
[57] S. Jinno, M. Kanasaki, M. Uno, R. Matsui, M. Uesaka, Y. Kishimoto, and Y. Fukuda, Plasma Phys. Controlled Fusion **60**, 044021 (2018).
[58] A. S. Pirozhkov *et al.*, Opt. Express **25**, 20486 (2017).
[59] H. Kiriyama *et al.*, Opt. Lett. **43**, 2595 (2018).